

The role of soil amendments in limiting the leaching of agrochemicals: Laboratory assessment for copper sulphate and dicamba

Original

The role of soil amendments in limiting the leaching of agrochemicals: Laboratory assessment for copper sulphate and dicamba / Granetto, M., Bianco, C., Tosco, T.. - In: JOURNAL OF CLEANER PRODUCTION. - ISSN 0959-6526. - ELETTRONICO. - 474:(2024). [10.1016/j.jclepro.2024.143532]

Availability:

This version is available at: 11583/2994765 since: 2025-01-07T09:53:47Z

Publisher:

Elsevier Ltd

Published

DOI:10.1016/j.jclepro.2024.143532

Terms of use:

This article is made available under terms and conditions as specified in the corresponding bibliographic description in the repository

Publisher copyright

Elsevier postprint/Author's Accepted Manuscript

© 2024. This manuscript version is made available under the CC-BY-NC-ND 4.0 license
<http://creativecommons.org/licenses/by-nc-nd/4.0/>. The final authenticated version is available online at:
<http://dx.doi.org/10.1016/j.jclepro.2024.143532>

(Article begins on next page)

1 The role of soil amendments in limiting the leaching of
2 agrochemicals: laboratory assessment for copper sulphate
3 and dicamba

4 Monica Granetto, Carlo Bianco, Tiziana Tosco*

5 *Department of Environmental, Land and Infrastructure Engineering (DIATI), Politecnico di Torino,*
6 *Corso Duca degli Abruzzi, 24, 10129, Turin, Italy*

7 * *Corresponding author: tiziana.tosco@polito.it*

8

9 Submitted to Journal of Cleaner Production

10

11 **Abstract**

12 Agriculture is among the major contributors to soil and groundwater pollution, primarily through the
13 widespread leaching of pesticides and fertilizers from crops, as well as accidental releases from point sources.
14 Therefore, alongside restrictions on the use of highly soluble agrochemicals and enhanced application
15 guidelines, there is a significant demand for low-impact and cost-effective solutions aimed at reducing the
16 mobility of agrochemicals in the soils. This study evaluates the potential of soil amendments—commonly
17 used to enhance soil structural properties, water holding capacity, and fertility—to also absorb highly soluble
18 pesticides, thereby controlling their leaching into the subsoil. Specifically, zeolite, biochar, and milled corncob
19 were examined in laboratory tests under static (batch tests) and dynamic (column leaching tests) conditions
20 to assess their effectiveness in adsorbing two widely used pesticides, copper sulphate and dicamba. Batch
21 adsorption tests were performed using the amendments as pure materials and in mixtures with sand at
22 various application rates (1 to 20% by weight). The highest affinity to copper sulphate was recorded for
23 biochar, while dicamba exhibited a higher affinity to corncob, thanks to its higher content of organic carbon.
24 Column leaching tests, performed at an amendment application rate of 5%, confirmed the different affinity
25 observed in batch tests among pesticides and amended soil. Less than 2% of copper sulphate leached out
26 from biochar- and zeolite-sand columns, while a recovery of 10% and 56% was observed for the corncob-
27 sand mixture and for pure sand, respectively. Dicamba leaching from biochar- and corncob-sand columns
28 was halved compared to pure sand. In conclusion, the tested soil amendments resulted highly effective in
29 reducing pesticide leaching, opening the way for their possible applications in agriculture to reduce or
30 prevent both diffuse and punctual contamination.

31

32 **Keywords**

33 Soil amendments; Zeolite; Biochar; Corncob; Pesticide leaching; Pesticide sorption

34 **Highlights**

35 Biochar and corncob show high affinity to dicamba and limit its leaching in lab tests

36 Zeolite-amended sand highly retain Cu sulphate and retention is partly irreversible

37 Unprocessed agricultural waste can effectively control leaching of organic pesticides

38

39 **Introduction**

40 Preserving the high quality of surface water and groundwater represents a current global challenge.
41 Agriculture, along with urban and industrial activities, is among the major pollution sources (Sethi and Di
42 Molfetta, 2019), including both diffuse emissions associated with excessive load of nutrients (in particular
43 phosphorus and nitrogen), pesticides and pharmaceuticals (Dordio and Carvalho, 2013), and accidental spills
44 at well-localized contamination roots (e.g. storage vessels or sprayer tanks, parking or loading areas, etc.)
45 (Ritter, 1988). Several technologies are currently available to manage point source releases and treat
46 collected streams of contaminated water, similar to those applied to industrial or civil effluents. Conversely,
47 controlling contaminant spread from diffuse sources is an intrinsically challenging target. To this aim, soil
48 amendments, in particular processed or raw agricultural waste (e.g. sawdust, mowing, biochar, etc.) and
49 minerals (e.g. zeolites) show good potential (Ahmad et al., 2014; Sud et al., 2008). Their effectiveness in
50 adsorbing and/or immobilizing organic and inorganic contaminants is already exploited in industrial
51 wastewater treatments and remediation of contaminated soils and sediments (Cao et al., 2011; Ghosh et al.,
52 2011). Conversely, in the agricultural sector, their primary use is currently as soil quality improvers, to
53 increase soil water retention capacity and control fertilizer release to plants (Diacono and Montemurro,
54 2010). Surprisingly, little attention has been devoted so far to their potential interactions with pesticides, and
55 more in general to limit contaminant release from agricultural sources (Kookana et al., 2011). Among the
56 limited literature available on this topic, notable findings include the biochar capacity to increase glyphosate
57 adsorption (with a partition coefficient 33% higher in biochar-amended soil than in untreated soil) (Kumari
58 et al., 2016) and the ability of Ca-hydroxide, Ca-bentonite, and natural zeolites to significantly increase the
59 copper immobilization compared to control soil (Lahori et al., 2017). Moreover, the leaching potential of
60 fipronil, a broad spectrum insecticide, was reduced by 97% in coarse sand amended with cereal straw,
61 compared to the unamended soil (Joshi et al., 2016). In this framework, this study intends to advance
62 knowledge on the role of soil amendments in controlling leaching of soluble agrochemicals.

63 Among adsorbents derived from agricultural waste, biochar, produced through pyrolysis of plant residues, is
64 the most known and used soil amendment. Its porous structure and surface properties render it an effective,

65 low cost material for removal of both organic (Tong et al., 2019) and inorganic compounds (Liu et al., 2022).
66 Similar advantages could be obtained also with mineral amendments like zeolites, whose exploitation in
67 agriculture increased in the last two decades (Mondal et al., 2021). Zeolites, sometimes after surface
68 modification, are often used in industrial wastewater treatments in deep bed filtration, and as soil
69 amendments for nutrients adsorption and controlled release (Ferretti et al., 2020; Wang and Wang, 2022).
70 However, only a few studies investigated their adsorption capacity toward agricultural contaminants such as
71 pesticides (Cataldo et al., 2021).

72 Despite the good performance of biochar and zeolites as adsorbents, their production processes (either
73 biochar pyrolysis or zeolite mining), milling and surface functionalization require non negligible energy input.
74 Consequently, in the name of a higher sustainability, perspective soil amendments produced from
75 agricultural waste with minimal energy demand would be highly desired. Milled corncob, with its large
76 availability and highly porous structure, is a promising option. It is currently exploited mainly for its high
77 energy content and as a source for biochar production, but to the authors' knowledge no previous study is
78 available on the efficacy of unprocessed corncob as an adsorbent. For this reason, it has been selected along
79 with biochar and zeolite to be investigated in this study.

80 Copper sulphate and dicamba, both characterized by high solubility and thus leaching potential, were studied
81 in this work as representative of, respectively, inorganic and organic pesticides. Copper, broadly used as
82 fungicide in organic agriculture, is among the priority pollutants categorized by USEPA. Copper leaching is
83 influenced by the precipitation intensity and duration, the chemistry of infiltrating water (ionic strength, pH),
84 and the presence and dynamics of dissolved organic matter (DOM), which has a high affinity with copper
85 (Aldrich et al., 2002). High infiltration was reported in sandy soils, with 47.9% of copper leaching from
86 columns spiked with 600 mg kg⁻¹ of Cu (Bakshi et al., 2014). Dicamba, an herbicide targeting broadleaf weeds
87 in crops like maize and sorghum, is highly soluble in water, with consequent high leaching potential (Granetto
88 et al., 2022). Its use in conjunction with 2,4-D has increased in USA since 2002 in response to the notable rise
89 in the number of herbicide-resistant weed biotypes (Hoy et al., 2015). Moreover, the introduction of

90 dicamba-resistant crops, such as soybeans and cotton, in Brazil (CTNBio, 2023) and other parts of the world,
91 suggests an overall increase in the application of this herbicide in the next years (Aguiar et al., 2023).

92 This research presents laboratory studies on the potentiality of soil amendments in limiting the leaching of
93 soluble pesticides in static (batch tests) and dynamic conditions (column leaching tests), elucidating the
94 dependence of adsorption mechanisms and removal efficiency on morphology, composition and physical-
95 chemical properties and application ratio of the amendments. Despite the laboratory scale of the study, a
96 few preliminary conclusions were drawn in view of a full-scale application of the studied amendments for
97 pesticide immobilization.

98

99

100 **Materials and methods**

101 ***Materials***

102 Three natural amendments were supplied by local producers, including biochar (Ronda Engineering; nominal
103 size < 5mm; source: pyrolysis at 700 °C of untreated woodworking waste), zeolite (Zeocel Italia; nominal size:
104 0.6-2mm; nominal composition: 70±5% chabazite, 2±1 % phillipsite, 5±2% sanidine, 3±1% augite, 2±1% illite),
105 and corncob (Agrindustria; nominal size: 50% 180-610µm and 50% 610-850µm; source: fibrous part of the
106 corn ear after extraction, drying and milling).

107 Silica sand (Dorsilit 8, Dorfner, Germany; d_{10} , d_{50} and d_{90} equal respectively to 0.415, 0.45 and 0.5 mm) was
108 used to mimic the soil structure, as pure material or mixed with the amendments. The cleaning procedure is
109 detailed in Beryani et al (2022). The following chemicals were used: copper sulphate pentahydrate
110 $\text{CuSO}_4 \cdot 5\text{H}_2\text{O}$ (Scharlab, Spain, purity > 99.5%), dicamba (Alfa Chemistry, US, purity > 99.5%), citric acid (Chem
111 Lab, Belgium, purity > 99.5%), trisodium citrate dehydrate (Supelco, ACS grade), Zincon (Alfa Aesar), HCl
112 (Merck EMSURE, ACS grade) and NaOH (Honeywell Fluka, ACS grade).

113

114 ***Characterization of the amendments and amendment-sand mixtures***

115 Zeolite and biochar samples were hand-crushed in a ceramic mortar prior use and sieved to discard the
116 fraction larger than 2mm. Corncob was not further milled since already provided in adequate size by the
117 producer. Particle size distribution (PSD) was measured via dry sieving for all samples. Particle shape and
118 elemental chemical composition were investigated using SEM-EDS microscopy (JEOL, Japan). To this aim, air-
119 dried samples were deposited on a stub using carbon (zeolite) or aluminium (biochar and corncob) tape, to
120 avoid interferences of the tape composition with EDS elemental peaks. Powder X-Ray diffraction (Rigaku
121 SmartLab SE) was performed on grounded samples using a CuK α radiation source ($\lambda = 1.54 \text{ \AA}$) operating at
122 40 kV and 30 Ma with scan range 5°-90° and scan step of 0.01°. Particle density was determined applying a
123 modified liquid pycnometer (BLAUBRAND, type Gay-Lussac, volume of 50cm³, calibrated according to DIN
124 ISO3507) method proposed by Heiskanen (Heiskanen, 1992).

125 The three amendments were then added separately to the sand at different application rates (1–2–5–10–
126 20% mass fraction) and hand-mixed up to complete homogenization. Bulk density, water holding capacity,
127 pH and salt content of pure amendments, pure sand and of the mixtures were determined according to the
128 European Biochar Certificate (EBC) guidelines for sustainable biochar production (Schmidt, 2015). Further
129 details are provided in paragraph 1 in Supporting Information.

130

131 ***Batch adsorption tests***

132 Adsorption tests were performed in 50 ml sealed glass vials, prepared by adding 2.5 g of solid material (pure
133 sand, pure amendment or a mixture of the two) to 25 ml of pesticide solution ranging 124 to 624 mg/l for
134 copper sulphate and 250 to 1500 mg/l for dicamba, corresponding to the application ranges commonly used
135 in agriculture for the two compounds. For each pesticide, six different initial concentrations were tested in
136 the respective range. The vials were continuously mixed with an overhead shaker (Rotax 6.8, Velp Scientifica,
137 Italy) at 15 rpm for 24 hours to ensure equilibrium between liquid and solid phases. The contact time was

138 selected based on kinetic adsorption tests, performed using the same experimental procedure at the
139 maximum concentration of the two pesticides in contact with the pure amendments (results reported in
140 paragraph 2 in Supporting Information). After 24 h, the samples were centrifuged at 6000 rpm for 20 mins
141 (Neya 16 centrifuge, REMI, India) and filtered with a PTFE syringe filter with 0.45 μm mesh to remove
142 suspended colloids. The supernatants were then analysed for residual copper or dicamba concentrations: a
143 colorimetric method, described in paragraph 3 in Supporting Information, was adapted from Ghasemi et al.
144 (2003) for copper, while dicamba was directly measured with Uv-VIS spectrophotometer (Specord S600,
145 Analytic Jena, Germany) at 280.5 nm (Figure S3-3). Given the concentration in liquid phase and the liquid
146 volume, the concentration in solid phase was calculated through mass balance.

147 The experimental results were modelled with Freundlich and Langmuir isotherms. The Freundlich model,
148 suitable for adsorption on heterogeneous surfaces (Vadivelan and Kumar, 2005), was expressed as

$$149 \quad s_{eq} = K_f C_e^{1/n} \quad (\text{eq. 1})$$

150 where s_{eq} is the adsorbed concentration [-] in equilibrium with the liquid concentration C_e [ML^{-3}], K_f is the
151 adsorption capacity [$\text{M}^{-1/n} \text{L}^{3/n}$] and $1/n$ is the Freundlich constant [-], being $1/n < 0.1$ for strongly favourable
152 adsorption, $0.1 < 1/n < 0.5$ for favourable adsorption, $1/n > 0.5$ for unfavourable adsorption.

153 The Langmuir model, suitable to describe monolayer adsorption (Liu, 2006), was expressed as

$$154 \quad s_{eq} = \frac{q_{max} L C_e}{1 + L C_e} \quad (\text{eq. 2})$$

155 where q_{max} is the maximum adsorption capacity [-] and L the Langmuir adsorption coefficient [$\text{L}^3 \text{M}^{-1}$].

156 In order to shade further light on adsorption mechanisms, the zeta potential of biochar, zeolite and corncob
157 diluted to 1 g/l in 3 mM NaCl solution was measured at varying pH (modified by dropwise addition of 50 mM
158 HCl or NaOH) using Dynamic Light Scattering (Malvern, Zetasizer NANO ZSP).

159

160

161 ***Column leaching tests***

162 Copper and dicamba leaching tests were performed in glass columns (inner diameter 4.1 cm) packed
163 with 320 g of dry sand or of a sand-amendment mixture at 5% application rate. For the mixtures, 16 g of
164 water were added prior packing to allow a slight cohesion between sand and amendment, thus avoiding
165 layering of the two materials during column filling. Column preparation included the following steps: (i) the
166 wet mixture was introduced in small amounts (~20 g) and compacted with a pestle layer by layer; (ii) upward
167 flow (0.2 ml/min) was established until complete saturation; (iii) the column length (~18 cm) was measured,
168 and the column weighted for saturated water content determination. The columns were then left draining
169 by gravity until field capacity was reached. Unsaturated downward flow (0.4 ml/min, corresponding to an
170 infiltration rate of 0.028 cm/min) was then established. A tracer test was performed injecting KBr at constant
171 concentration and the breakthrough electrical conductivity curve was recorded. The unsaturated water
172 content, unsaturated pore volume (PV) time, saturated hydraulic conductivity, and dispersivity were
173 determined via least-squares fitting of the breakthrough curve (BTC) to the classical advection-dispersion
174 equation in unsaturated porous media (paragraph 4 in SI) using Hydrus 1D (Simunek et al., 2013).

175 After the tracer test, a copper sulphate or dicamba solution (depending on the test) was injected for at least
176 7.5 h at constant concentration of 624 mg/l or 1500 mg/l, respectively, followed by a flushing with deionized
177 water for 7.5 h. The column outflow was collected using a fraction collector and samples analysed for copper
178 and dicamba with the same methods used for adsorption tests.

179 At the end of the tests, the columns were extruded and dissected to determine copper and dicamba profiles.
180 Copper was extracted from the solid by using a modified version of the sequential extraction method
181 proposed by Silveira (Silveira et al., 2006), including the following steps: (i) addition of 0.1 M CaCl₂ and mixing
182 for 24h to promote ion exchange, (ii) addition of 1M NaOAc (Carlo Erba, purity > 99%) and mixing for 5h for
183 the extraction of Cu(II) adsorbed on grain surface, and (iii) addition of NaOCl (Carlo Erba, solution at 30%) at
184 90°C for 2h to promote release from the organic matter. Cu precipitated in oxide/hydroxide form is expected
185 not to be recovered. Dicamba was extracted in one step using acetonitrile:CaCl₂ 10 mM 70:30 w/w with
186 continuous mixing for 24h. All suspensions were centrifuged at 6000 rpm for 20 min before the analysis.

187 Copper and dicamba BTCs were modelled with Hydrus 1D (Simunek et al., 2012) using a two-site
 188 adsorption equilibrium model, having one site characterized by instantaneous adsorption (eq. 4) and the
 189 other one by kinetic adsorption (eq. 5 and 6):

$$190 \quad \frac{\partial \theta c}{\partial t} + \rho \frac{\partial s^e}{\partial t} + \rho \frac{\partial s^k}{\partial t} = \frac{\partial}{\partial z} \left(\theta D \rho \frac{\partial c}{\partial z} \right) - \frac{\partial q c}{\partial z} - \varphi \quad (\text{eq. 3})$$

$$191 \quad s^e = f_e F(c) \quad (\text{eq. 4})$$

$$192 \quad \rho \frac{\partial s^k}{\partial t} = \alpha_k \rho (s_e^k - s^k) - \varphi_k \quad (\text{eq. 5})$$

$$193 \quad s_e^k = (1 - f_e) K_d c \quad (\text{eq. 6})$$

194 where s^e is the solute concentration adsorbed on the instantaneous (equilibrium) adsorption site expressed
 195 as mass of adsorbed solute per unit mass of solid [-], $F(c)$ is the corresponding adsorption isotherm (linear,
 196 Langmuir, etc.), f_e is the fraction of exchangeable sites in equilibrium with the liquid phase [-], s^k is the
 197 concentration adsorbed on the kinetic (non-equilibrium) adsorption site [-] and s_e^k is the corresponding
 198 adsorbed concentration at equilibrium for the kinetic adsorption site [-] expressed by the linear isotherm of
 199 eq. 6, α_k is the first order rate constant of the kinetic site [T^{-1}], K_d is the partition coefficient for the kinetic
 200 site [$L^3 M^{-1}$], φ and φ_k are the sink/source terms accounting for generic reactions [$ML^{-3} T^{-1}$]. The total adsorbed
 201 concentration is $s = s^e + s^k$.

202

203 **Results and discussion**

204 ***Characterization of the amendments and amendment-sand mixtures***

205 The milled biochar showed a highly heterogeneous morphology (Figure 1a), with larger particles exhibiting a
 206 highly intra-porous structure, and smaller ones characterized by an elongated, flat shape. The PSD analysis
 207 indicated d_{10} , d_{50} and d_{90} equal to 0.15, 0.7 and 1.9 mm respectively (Figure S5-1). The XRD pattern (Figure
 208 1b) showed the typical biochar composition, including mainly aromatic hydrocarbons and graphite-like
 209 carbon structures (Gao et al., 2020). The humped trend in the region $15^\circ < \theta/2\theta < 30^\circ$ is due to the amorphous

210 carbonaceous structure resulting from pinewood pyrolysis. The high peak at 26.5° can be associated with
211 pyrolysis of inorganic impurities, mainly graphite (Mohan et al., 2018), while additional peaks at 29°, 36°, 39°,
212 44° and 48° can be associated with superficial Ca-based compounds such as CaCO₃ and CaO (Tran et al., 2015;
213 Waqas et al., 2021).

214 Hand-milled zeolite showed a distinctly cubic shape, with well-defined angles and smoothed faces due to
215 mechanical crushing (Figure 1c), and particle size lower than 1 mm (d_{10} , d_{50} and d_{90} respectively equal to 0.07,
216 0.4 and 0.9 mm, Figure S5-2). The XRD pattern (Figure 1d) was consistent with that of Ca-chabazite type
217 zeolite, characterized by a stronger diffraction response at $\theta/2\theta < 15^\circ$ compared to K-chabazite, as reported
218 by previous crystallographic studies (Leyva-Ramos et al., 2008). This is confirmed by EDS results (Figure S5-
219 4), reporting the presence of Ca (3.2% on average). Peaks in the XRD spectrum other than those characteristic
220 of chabazite were identified at $\theta/2\theta = 23.3^\circ - 30.4^\circ$. A good agreement was found with sanidine at 23.3°,
221 27.5°, 27.9° and 29.7°, with illite at 29.9° and 34.14° and with augite at 27.5°, 39.7°, 30.4° and 35.5°,
222 coherently with the nominal sample composition and with previous studies (Ramos et al., 2015).

223 Corncob (not further milled) showed a higher heterogeneity and irregularity in terms of both PSD (d_{10} , d_{50}
224 and d_{90} equal to 0.2, 0.55 and 0.85 mm, Figure S5-3) and morphology compared to biochar and zeolite. The
225 SEM analysis (Figure 1e) identified the presence of elongated particles interspersed with more compact,
226 jagged ones. The first ones could be attributed to the central pitch part of corncob, the latter to the external
227 glume and wood ring. The XRD pattern (Figure 1f) denoted a highly amorphous lignocellulose material (in
228 particular alfacellulose) identified by two peaks at $\theta/2\theta = 16^\circ$ and 22° (Menezes et al., 2017). Crystalline
229 peaks at 36° and 44° could be traced back to Ca-containing impurities on corncob surface.

230 Figure 2 reports the results of the sand-amendment mixture characterization (bulk density, water holding
231 capacity, electrical conductivity and pH) obtained following the EBC guidelines for sustainable biochar
232 production. The grain density, measured with a liquid pycnometer, resulted in the following trend: sand (2.6
233 g/cm³) > zeolite (2.35 g/cm³) > biochar (1.6 g/cm³) > corncob (1.52 g/cm³). The amendment addition to the
234 sand significantly affected the bulk density of columns dry-packed with the mixtures (Figure 2a), which

235 decreased linearly from 1.53 g/cm³ for pure sand with increasing amendment application ratio, reaching
236 1.33, 1.07 and 0.81 g/cm³ for 20% application rates of zeolite, corncob and biochar, respectively. The highest
237 bulk density reduction (45.3%) was obtained with biochar, even though the lowest grain density was
238 measured for corncob, suggesting that the bulk density of the mixtures was not a mere weighted mean of
239 the densities of sand and amendment but, rather, was significantly affected by the amendment particle
240 shape. The theoretical porosity corresponding to the measured bulk density (Figure S5-5) increased from
241 0.41 for pure sand to 0.48, 0.52 and 0.66 for zeolite, corncob and biochar, respectively, at 20% application
242 rate, thus confirming the beneficial effect of amendments (and in particular of biochar and corncob) in terms
243 of reduced bulk density and increased porosity, and consequently reduced soil compaction, higher aeration
244 and potentially lower risk for soil erosion.

245 The water holding capacity (WHC) increased with increasing the amendment application rates (Figure 2b),
246 and the general observed WHC trend was corncob>biochar>zeolite. At the highest application rates (20%),
247 WHC of 0.34, 0.54 and 0.55 g/g were measured respectively for zeolite-, corncob- and biochar-sand mixtures,
248 corresponding to a WHC increase of 72%, 172% and 177% compared to pure sand. For biochar, both intra-
249 porosity, inter-porosity and the highly irregular surface morphology are expected to have positively affected
250 the biochar-sand mixture WHC (Liu et al., 2017; Verheijen et al., 2019). Similar considerations could be drawn
251 for corncob-sand mixtures, even though no previous literature is available on the characterization of
252 unprocessed corncob as soil amendment. Conversely, the (limited) effect of zeolite on the WHC of the
253 mixtures is mainly attributable to a decrease in particle size, and consequently increase in capillary water
254 retention (Ibrahim and Alghamdi, 2021).

255 The water electrical conductivity of the pure amendments in contact with water was equal to 29, 165 and
256 1015 $\mu\text{S}/\text{cm}$ for zeolite, biochar and corncob, respectively. The conductivity of the amendment-sand mixtures
257 increased significantly with increasing the amendment application rates, except for zeolite-containing
258 samples, which did not show any significant trend (Figure 2c). Conversely, the high conductivity of pure
259 biochar and corncob denoted a high propensity to free and exchange ions in solution. It is worth to mention
260 that higher values of conductivity, and so salt content, could lead both to a higher potential for ions exchange

261 and ionic species adsorption, but also to a reduced germinability and damage to crop due to induced salt
262 stress (Buss et al., 2016).

263 The pH value of the pure materials in contact with water was 7.5, 8.4, 6.7 and 4.7 for sand, biochar, zeolite
264 and corncob, respectively. Coherently, the mixtures showed slightly alkaline pH for biochar, nearly neutral
265 for zeolite and acidic for corncob (Figure 2d). The biochar-sand mixture pH was close to pure biochar pH at
266 all application rates, suggesting that biochar is able to buffer sand, contrary to corncob and zeolite, which
267 showed decreasing pH with increasing application rates.

268

269 ***Adsorption tests***

270 ***Copper sulphate***

271 The copper sulphate adsorption isotherms for the mixtures are reported in Figure 3a-c as adsorbed
272 concentration s_{eq} (i.e. adsorbed $CuSO_4$ mass over the total mass of adsorbent, i.e. sand + amendment) against
273 $CuSO_4$ residual concentration in liquid phase at equilibrium. Adsorption on pure sand was minimal compared
274 to the mixtures. The adsorption capacity followed the trend biochar>zeolite>corncob. Biochar isotherms
275 showed a trend toward saturation (Figure 3a) for application rates lower than 5%. For rates higher than 10%
276 the same trend can be hypothesized, even though the plateau was not reached since the tests were
277 performed exploring the environmentally-relevant range of $CuSO_4$ concentrations. A similar saturative trend
278 was shown by zeolite-sand mixtures (Figure 3b) but not by corncob-amended sand (Figure 3c).

279 The experimental isotherms were least-squares fitted to the Langmuir and Freundlich models. The model
280 parameters are reported in Supporting Information in Table S6-1 and their trends as a function of the
281 amendment application rates are reported in Figure 4. As a general rule, both models resulted in very high
282 R^2 values for most isotherms, with a few exceptions. A slightly better fitting with the Langmuir model
283 compared to Freundlich (see R^2 values) suggests a monolayer adsorption mechanism on a homogeneous
284 adsorbent surface, coherently with other studies on $CuSO_4$ interaction with various adsorbents (Wang et al.,
285 2012; Zand and Abyaneh, 2020).

286 Biochar showed a general better fitting with the Langmuir model compared to the Freundlich one,
 287 particularly for rates < 20%. Adsorption was unfavourable ($1/n \geq 0.5$) for biochar rates $\geq 20\%$, and favourable
 288 ($1/n < 0.5$) for rates < 10% (Figure 4a). Conversely, the Freundlich adsorption coefficient K_f showed a bimodal
 289 trend in the range 0.09 to 0.74 g l^{1/n} with a peak at application rate of 5% (Figure 4b). Increasing q_{max} with
 290 increasing application rate was also observed (Figure 4c). Zeolite showed a very good fitting for both
 291 Freundlich and Langmuir isotherms for application rates from 1% to 20%, with slightly higher R² values for
 292 the Freundlich model at medium-to-high application rates, and particularly for rates > 5%. The fitted values of
 293 $1/n$ increased with increasing application rates in the range 0.15-0.3, thus suggesting that copper adsorption
 294 on zeolite is a favourable process (Figure 4a). As for corncob, the Langmuir model showed a general better
 295 fitting compared to the Freundlich one, with saturation concentration q_{max} significantly lower than those
 296 obtained for biochar (Figure 4c).

297 To further investigate the adsorption capacity and mechanisms, the isotherms were reported also in terms
 298 of adsorbed CuSO₄ normalized to the mass of amendment (i.e. excluding sand), $s_{eq,norm}$, calculated as

$$299 \quad s_{eq,norm} = \frac{s_{eq} - s_{eq,AR=0\%}(1 - AR)}{AR}$$

300 where $s_{eq,AR=0\%}$ is the adsorbed concentration measured in the absence of amendment (i.e. when sand is the
 301 only solid in the batch). An unexpected trend of the results was obtained (Figures 3d-f): with decreasing
 302 application rates, $s_{eq,norm}$ increased for all tested materials. This suggests that adsorption is more efficient
 303 in the presence of a low adsorbent content in the solid fraction, even though the adsorption on sand grains
 304 is minimal.

305 In general, the main expected mechanisms of CuSO₄ removal from water include surface adsorption (due to
 306 electrostatic attraction and ion exchange), and precipitation of Cu oxides and hydroxides at favourable
 307 hydrochemical conditions (Tan et al., 2015; Zhao et al., 2020). For both mechanisms, pH plays a key role. The
 308 pH was acidic in all our tests due to the presence of CuSO₄ in solution, and was slightly affected by the
 309 amendment application rates (Figure S6-1): in particular, pH was close to 5 for pure sand and increased with
 310 increasing both zeolite and biochar application rate toward plateau values of approximately 6 and 7,

311 respectively, but decreased toward approximately 4.5 for corncob-sand mixtures (coherently with the more
312 acidic pH of corncob). Concerning copper precipitation, Jiang et al. (Jiang et al., 2016) indicate that, for acidic
313 CuSO_4 solutions in contact with biochar, the formation of insoluble $\text{Cu}(\text{OH})_2$ is expected starting from pH
314 above 6. Thus, the pH values of our tests would explain the limited Cu removal observed for pure sand and
315 corncob (Figure 3f), and the higher one for zeolite and biochar (Figures 3d and 3e), even though the pH values
316 measured for zeolite- and biochar-sand mixtures are not high enough to suggest a predominance of
317 precipitation as removal mechanism. The pH influences the surface charge of the adsorbent and thus the
318 surface adsorption due to electrostatic attraction toward dissolved copper ions. Zeta potential, which can be
319 used as an indirect measurement of surface charge, was negative for all amendments in our tests (Figure S5-
320 6), and decreased with increasing pH, suggesting a higher affinity of the amendments to the copper cations
321 at higher pH. Again this trend would explain the corncob isotherms but not those obtained for zeolite and
322 biochar. Consequently, other properties controlling surface adsorption are likely to play the major role in our
323 tests. Among them, the specific surface area of the amendment is likely the parameter controlling adsorption
324 capacity. It was observed that during the adsorption experiments the particle size of the amendment was
325 reduced: optical microscope analysis of corncob particles before and after the adsorption tests evidenced a
326 clear decrease in size (Figure S6-2 in Supporting Information); particle size distributions obtained via image
327 processing (ImageJ, National Institutes of Health, US) showed that the difference is more pronounced at low
328 application rate (5%) and negligible at the highest application rate (20%) (Figure S6-3). This can be explained
329 by sand acting as ball milling, thus reducing amendment particle size during mixing with the overhead shaker
330 (Shan et al., 2016): the higher the sand content in the sample, the more effective the milling. Higher copper
331 loading potential at decreasing particle size was also reported previously for biochar, and was attributed to
332 a larger surface area available and easier accessibility to pores for finer adsorbents (Zou et al., 2006).

333

334 ***Dicamba***

335 The dicamba adsorption isotherms (Figure 5) show a higher overall adsorption capacity for corncob
336 and biochar, followed by zeolite. For all tested materials, the removal efficiency increased with increasing

337 application rate, similarly to what observed for CuSO₄. The contribution of sand to dicamba adsorption is
338 minor, even though not negligible, compared to the three amendments (see black dotted isotherms in Figure
339 5). For biochar- and corncob-sand mixtures (Figures 5a and 5c), the isotherms showed an asymptotic trend
340 toward a saturation concentration for rates <10% and <5%, respectively. The saturative trend is further
341 evidenced when the isotherms are normalized to the mass of amendment (Figure 5d and f). Conversely,
342 zeolite isotherms were distinctly linear at all tested application rates, without any evident saturative
343 behaviour (Figures 5b and e). It is worth observing that the removal efficiency of pure zeolite is lower than
344 the other two pure amendments, but for low application rates (up to 2%) the removal efficiency of zeolite-
345 sand mixtures (Figure 5b) was comparable to or higher than the others. This is reflected by remarkably higher
346 normalized isotherms for zeolite at low application rates (Figure 5e).

347 The overall increasing adsorption efficiency of the adsorbents with decreasing application rates, as
348 evidenced in Figures 5d-f, is in line with the results obtained for CuSO₄, and confirms the key role of sand-
349 mediated milling of the amendments in increasing the sorption efficiency in batch tests. However, the effect
350 of comminution alone is not sufficient to explain all the results reported in Figures 5d-f, and in particular the
351 overall reduced adsorption efficiency of biochar compared to corncob and zeolite. A key role in this sense is
352 likely played by pH: dicamba in solution exhibits an acidic behaviour (Azejjel et al., 2008), with pKa equal to
353 1.98 (Carrizosa et al., 2001). The dissociated dicamba molecule assumes a negative charge, that contrasts
354 with the negative surface charge of zeolite/biochar/corncob. Thus, the dicamba adsorption is favoured when
355 the compound is present in its molecular form, rather than when dissociated, and consequently at strongly
356 acidic pH. Figure S6-4 in Supporting Information reports the trends for the pH measured in batch tests as a
357 function of amendment application rates. For pure sand, the sample pH was 2.8, close to pKa. For all
358 amendments, the pH increased with increasing application rate. As for biochar, pH rapidly approached
359 neutrality for application rates higher than 5%, corresponding to a predominantly dissociated form of
360 dicamba and thus to a lower affinity of the molecule to the amendment. Correspondingly, biochar exhibited
361 the lowest normalized isotherms among the three tested materials (Figure 5d). For zeolite and corncob, the
362 pH remained close to 3 for application rates lower than 5%. Correspondingly, the normalized isotherms of

363 Figures 5e and f showed higher adsorbed concentrations at low application rates compared to biochar. This
364 finding suggests that, along with the optimal adsorbent milling obtained at low application rates, also pH
365 played a fundamental role in controlling dicamba adsorption potential.

366 The modelling of dicamba isotherms with Langmuir and Freundlich equations (coefficients in Table
367 S6-2 in Supporting Information, trends with application rates in Figure 6) showed a good fitting for both
368 models and for all the three materials, with slightly higher R^2 values for the Langmuir model. For all zeolite-
369 sand mixtures, linear adsorption was confirmed, being always $1/n > 1$ (Figure 6a). The Freundlich adsorption
370 coefficient K_f slightly decreased for biochar- and corncob-sand mixtures, and increased for zeolite-sand
371 mixtures, with increasing application rate (Figure 6b). Corncob and biochar showed $1/n < 1$, increasing toward
372 the unit with increasing application rates, thus suggesting adsorption of pseudo-linear type.

373

374 ***Leaching tests***

375 ***Column hydrodynamic characterization***

376 The hydrodynamic parameters of the columns in leaching tests in unsaturated conditions are reported in
377 Table 1. A higher water content θ for the biochar-sand column compared to others was expected according
378 to the higher amendment WHC, higher biochar porosity and heterogeneous particle structure. The saturated
379 hydraulic conductivity K_s was higher for pure sand and decreased progressively for corncob-, zeolite-, and
380 biochar-sand mixtures, in accordance with previous literature (Sarabi and Sepaskhah, 2012; Yan et al., 2021).
381 Conversely, the hydrodynamic dispersivity α was similar in all tests.

382

383 ***Copper sulphate leaching tests***

384 Figure 7a reports the breakthrough curves of copper sulphate in the four columns as a function of the injected
385 unsaturated pore volumes (PVs). In general, the ability of the amendment-sand mixture to retain CuSO_4
386 followed the order sand < corncob-sand < zeolite-sand / biochar-sand mixtures. In pure sand, a relevant delay

387 in the breakthrough of CuSO_4 was observed, with $C/C_0 > 0$ after 1.5 PVs, suggesting the occurrence of
388 reversible equilibrium adsorption. A fairly constant concentration $C/C_0 \sim 0.9$ was then measured for the entire
389 duration of the injection step, indicating the occurrence, in parallel, of reversible equilibrium adsorption and
390 kinetic irreversible adsorption or of precipitation. For zeolite and biochar, an almost null breakthrough was
391 observed, with no CuSO_4 release even during post-flushing with deionized water, thus suggesting that CuSO_4
392 was irreversibly adsorbed and/or precipitated in the tested hydrochemical conditions. Negligible
393 breakthrough was observed also for the sand-corncob column for 4.5 PVs, followed by a limited
394 breakthrough. However, during flushing a significant desorption occurred, indicating in this case a weaker
395 and partly reversible interaction between Cu and corn cob.

396 Relevant additional information can be obtained from the profiles of retained concentration of CuSO_4 ,
397 obtained dissecting the columns at the end of the leaching tests (Figure 7b). An almost constant copper
398 concentration was detected along the vertical direction in pure sand (~ 0.09 mg/g) and for the corn cob-sand
399 mixture (~ 0.29 mg/g, except for the deepest 4 cm). It is worth noticing that in both tests a non-negligible
400 copper breakthrough concentration was measured at the end of injection, thus suggesting the two columns
401 reached saturation along the entire column (for sand) or at least in its upper part (for the corn cob-sand
402 mixture). Conversely, a different profile shape was observed for zeolite- and biochar-sand mixtures: in both
403 cases, a higher Cu concentration was retained in the first 6 cm and negligible concentrations in the deepest
404 part of the column, thus suggesting that biochar and zeolite have a much higher sorption capacity and column
405 saturation was not reached during the test.

406 A closer analysis of the percentage of Cu recovered in each step of the sequential extraction method (aimed
407 at recovering Cu aliquots retained due to different phenomena) provides additional information on the
408 retention mechanisms (Figure S7-1 in Supporting Information). In all tests, the highest recovery was obtained
409 in the first extraction step, aimed at promoting Cu(II) release via ion exchange. This predominance is
410 particularly evident for corn cob and biochar, confirming the higher ion exchange capacity of these
411 amendments compared to pure sand and zeolite. For the second extraction, aimed at releasing Cu adsorbed
412 on mineral surfaces, the highest recovery was obtained for pure sand, followed by zeolite-, biochar- and

413 corncob-sand mixtures, indicating a slightly higher affinity of Cu to sand compared to zeolite surface. In the
414 third extraction, aimed at extracting Cu adsorbed on the organic matter, the largest recovery percentage, as
415 expected, was obtained for corncob. In all tests, and particularly for zeolite- and biochar-sand mixtures, a
416 non-negligible fraction of Cu (Table 1) was not recovered at column outflow nor in the extraction procedure,
417 suggesting that Cu precipitation in the form of oxides/hydroxides (which cannot be extracted by none of the
418 methods adopted in the three steps) also partly occurred.

419 The breakthrough curve for pure sand was modelled using eq. 3 - 6 with one instantaneous (equilibrium)
420 adsorption site (eq. 4) following a Langmuir isotherm, and one kinetic adsorption site (eq. 5). The fitting was
421 satisfactory (Figure S7-2) with $R^2 = 0.91$. For the equilibrium site, the Langmuir parameters obtained were
422 $q_{\max} = 4.02 \cdot 10^{-1}$ mg/g and $L = 1.66 \cdot 10^{-3}$ l/mg, similar to the values obtained in batch tests for CuSO_4 adsorption
423 onto pure sand (Table S6-1). As for the kinetic site, $\alpha_k = 1.29 \cdot 10^{-3} \text{ min}^{-1}$ and $\varphi_k = 2.37 \cdot 10^{-3} \text{ min}^{-1}$ were
424 obtained. The fraction of instantaneous adsorption sites where adsorption f_e was equal to 0.42, in agreement
425 with the similar percentages of Cu recovery obtained in the first and second steps of the sequential extraction
426 method.

427

428 ***Dicamba***

429 Contrary to CuSO_4 leaching tests, dicamba showed a significant breakthrough in all tested columns,
430 corresponding to an overall lower affinity to the tested amendments (Figure 8a). No evident retardation was
431 observed for pure sand and zeolite-sand mixture, while breakthrough was retarded for biochar- and
432 corncorb-sand mixtures, with a retardation factor equal to 1.8 and 2.5, respectively. Beside retardation,
433 which suggests the occurrence of instantaneous equilibrium adsorption, all breakthrough curves also showed
434 a steady-state concentration plateau lower than the injected one, suggesting the concomitant occurrence of
435 kinetic adsorption. From a qualitative point of view, the affinity of dicamba for the sorbent materials
436 confirmed the same trend corncob>biochar>zeolite evidenced by batch tests, and by mass balances (Table
437 1).

438 Figure 8b reports the vertical profile of retained dicamba at the end of the leaching tests. The profile for the
439 corncob-sand mixture was not determined due to interference with other substances released by the
440 corncob matrix. As a general trend, higher adsorption was observed in the upper part of the columns, where
441 higher concentrations in pore water were present, even though concentrations are not negligible also at
442 higher depths. The non-negligible concentrations of adsorbed dicamba measured along the column at the
443 end of the test confirm the presence of two concurrent adsorption mechanisms (instantaneous and kinetic,
444 the second being partly irreversible) hypothesized based on breakthrough curves: if adsorption was totally
445 reversible, no significant retained concentration should have been measured, having breakthrough curves
446 reached negligible values at the end of all tests.

447 The breakthrough curves of all dicamba leaching tests were modelled assuming the same mechanisms used
448 for CuSO_4 (parameter in Table S7-1, modelled curves in Figure S7-3 in Supporting Information). The fitting
449 was visually satisfactory with $R^2 > 0.95$ for all tests except for the sand-corn-cob mixture. The first-order rate
450 constant for dissolved phase α_k was higher for sand and sand-zeolite mixtures compared to biochar- and
451 corn-cob-sand columns, suggesting that the latter materials reach faster equilibrium for the kinetic site
452 compared to biochar- and corn-cob-sand columns. Comparing batch and column equilibrium adsorption
453 parameters, and in particular the maximum adsorption capacity s_{\max} (Figure 9a), it can be observed that in all
454 cases the q_{\max} values obtained in batch were higher than those obtained in columns, but with the same trend,
455 likely due to the better and longer contact between adsorbents and dicamba solutions.

456

457 **Conclusions**

458 In this study, zeolite, biochar and corncob were used to adsorb and reduce the mobility in water and soil of
459 two pesticides, namely copper sulphate and dicamba. These amendments were mixed with silica sand at
460 different application rates. A general decrease in bulk density and a notable increase in water holding
461 capacity were observed with increasing application rates, particularly for biochar and corncob. This suggests
462 their higher potential for enhancing water storage in fields during drought conditions. Conversely, zeolite

463 showed minimal impact on both bulk density and water holding capacity. The addition of amendments also
464 significantly altered the pH. Thus, the physical and chemical effects of adding amendments to sand or soil in
465 crop fields must be taken carefully into account, particularly in the presence of plants and crops with specific
466 tolerance thresholds to salt/pH/soil humidity.

467 The ability of the different mixtures to adsorb pesticides were first tested in batch. The amendment initial
468 particle size distribution, application rate and the way of mixing used during adsorption test played crucial
469 roles in the adsorption tests. In particular, head-over-head mixing allowed a significant reduction of
470 amendment particle size due to friction with sand, thus enhancing adsorption rates, particularly at the lowest
471 application rates. This finding evidences the importance of a careful evaluation of the results of batch
472 adsorption tests, particularly when extrapolating their results to larger scales (column or field), due to the
473 high impact of the specific operating conditions on the results. Highly charged amendments, such as biochar
474 and zeolite, showed a higher affinity with copper, while dicamba was highly adsorbed by corncob due to its
475 high organic matter content. The Langmuir adsorption model best fitted the experimental results for both
476 copper sulphate and dicamba, suggesting a monolayer adsorption onto amendment surfaces.

477 Preliminary column leaching tests were conducted to assess the amendments' effects under hydrodynamic
478 conditions. The results confirmed the higher affinity of biochar and zeolite for copper sulphate, with
479 negligible leaching of copper from the column, compared to sand and sand-corn cob columns. For dicamba,
480 higher retardation factor and consequently higher retention were observed in the corncob-sand mixture. In
481 field conditions, this would result in longer retention of dicamba in the top soil, thus making its
482 biodegradation more favourable.

483 In conclusion, natural soil amendments can be used not only to improve the physical-chemical characteristics
484 of the soil, as currently practiced in some agronomic techniques, but also to enhance adsorption of pesticides
485 in the soil, thus limiting the spreading of both diffuse and local contaminations in agricultural settings. The
486 results of this study also highlight the potential benefits of combining multiple amendments at the field scale,

487 where diverse types of pesticides are applied, to limit the overall leaching of agrochemicals into deeper soil
488 and groundwater.

489 Cited literature

- 490 Aguiar, A.C.M. de, Silva, E.M.G. da, Barcellos Júnior, L.H., Paula, D.F. de, Souza, P.S.R. de, Guimarães, T.,
491 Ovejero, R.F.L., Palhano, M.G., Silva, A.A. da, Mendes, K.F., 2023. Sorption, leaching, and
492 degradation of dicamba in two Brazilian soils: A study into soil layers. *Crop Protection* 174, 106393.
493 <https://doi.org/10.1016/j.cropro.2023.106393>
- 494 Ahmad, M., Rajapaksha, A.U., Lim, J.E., Zhang, M., Bolan, N., Mohan, D., Vithanage, M., Lee, S.S., Ok, Y.S.,
495 2014. Biochar as a sorbent for contaminant management in soil and water: A review. *Chemosphere*
496 99, 19–33. <https://doi.org/10.1016/j.chemosphere.2013.10.071>
- 497 Aldrich, A.P., Kistler, D., Sigg, L., 2002. Speciation of Cu and Zn in Drainage Water from Agricultural Soils.
498 *Environmental Science & Technology* 36, 4824–4830. <https://doi.org/10.1021/es025813x>
- 499 Azejjel, H., Aatouf, N., Draoui, K., Rodriguez-Cruz, S., Sánchez-Martín, M., 2008. Influence of soil properties
500 on the adsorption of two ionisable herbicides by Moroccan soils. *Fresenius Environmental Bulletin*
501 17, 1627–1633.
- 502 Bakshi, S., He, Z.L., Harris, W.G., 2014. Biochar Amendment Affects Leaching Potential of Copper and
503 Nutrient Release Behavior in Contaminated Sandy Soils. *Journal of Environmental Quality* 43, 1894–
504 1902. <https://doi.org/10.2134/jeq2014.05.0213>
- 505 Beryani, A., Bianco, C., Casasso, A., Sethi, R., Tosco, T., 2022. Exploring the potential of graphene oxide
506 nanosheets for porous media decontamination from cationic dyes. *Journal of Hazardous Materials*
507 424, 127468. <https://doi.org/10.1016/j.jhazmat.2021.127468>
- 508 Buss, W., Graham, M.C., Shepherd, J.G., Mašek, O., 2016. Suitability of marginal biomass-derived biochars
509 for soil amendment. *Science of The Total Environment* 547, 314–322.
510 <https://doi.org/10.1016/j.scitotenv.2015.11.148>
- 511 Cao, X., Ma, L., Liang, Y., Gao, B., Harris, W., 2011. Simultaneous immobilization of lead and atrazine in
512 contaminated soils using dairy-manure biochar. *Environ Sci Technol* 45, 4884–4889.
513 <https://doi.org/10.1021/es103752u>
- 514 Carrizosa, M.J., Koskinen, W.C., Hermosin, M.C., Cornejo, J., 2001. Dicamba adsorption–desorption on
515 organoclays. *Applied Clay Science* 18, 223–231. [https://doi.org/10.1016/S0169-1317\(01\)00037-0](https://doi.org/10.1016/S0169-1317(01)00037-0)
- 516 Cataldo, E., Salvi, L., Paoli, F., Fucile, M., Masciandaro, G., Manzi, D., Masini, C.M., Mattii, G.B., 2021.
517 Application of Zeolites in Agriculture and Other Potential Uses: A Review. *Agronomy* 11, 1547.
- 518 Diacono, M., Montemurro, F., 2010. Long-term effects of organic amendments on soil fertility. A review.
519 *Agronomy for Sustainable Development* 30, 401–422. <https://doi.org/10.1051/agro/2009040>
- 520 Dordio, A., Carvalho, A.J., 2013. Constructed wetlands with light expanded clay aggregates for agricultural
521 wastewater treatment. *The Science of the total environment* 463–464, 454–61.
522 <https://doi.org/10.1016/j.scitotenv.2013.06.052>
- 523 Ferretti, G., Keiblinger, K.M., Faccini, B., Di Giuseppe, D., Mentler, A., Zechmeister-Boltenstern, S., Coltorti,
524 M., 2020. Effects of Different Chabazite Zeolite Amendments to Sorption of Nitrification Inhibitor
525 3,4-Dimethylpyrazole Phosphate (DMPP) in Soil. *Journal of Soil Science and Plant Nutrition* 20, 973–
526 978. <https://doi.org/10.1007/s42729-020-00184-3>
- 527 Gao, Y., Xiao, Y., Mao, K., Qin, X., Zhang, Yuan, Li, D., Zhang, Yanhui, Li, J., Wan, H., He, S., 2020.
528 Thermoresponsive polymer-encapsulated hollow mesoporous silica nanoparticles and their
529 application in insecticide delivery. *Chemical Engineering Journal* 383, 123169.
530 <https://doi.org/10.1016/j.cej.2019.123169>
- 531 Ghasemi, J., Ahmadi, S., Torkestani, K., 2003. Simultaneous determination of copper, nickel, cobalt and zinc
532 using zincon as a metallochromic indicator with partial least squares. *Analytica Chimica Acta* 487,
533 181–188. [https://doi.org/10.1016/S0003-2670\(03\)00556-7](https://doi.org/10.1016/S0003-2670(03)00556-7)

- 534 Ghosh, U., Luthy, R.G., Cornelissen, G., Werner, D., Menzie, C.A., 2011. In-situ Sorbent Amendments: A New
535 Direction in Contaminated Sediment Management. *Environ. Sci. Technol.* 45, 1163–1168.
536 <https://doi.org/10.1021/es102694h>
- 537 Granetto, M., Serpella, L., Fogliatto, S., Re, L., Bianco, C., Vidotto, F., Tosco, T., 2022. Natural clay and
538 biopolymer-based nanopesticides to control the environmental spread of a soluble herbicide.
539 *Science of The Total Environment* 806, 151199. <https://doi.org/10.1016/j.scitotenv.2021.151199>
- 540 Heiskanen, J., 1992. Comparison of three methods for determining the particle density of soil with liquid
541 pycnometers. *Communications in Soil Science and Plant Analysis* 23, 841–846.
542 <https://doi.org/10.1080/00103629209368633>
- 543 Hoy, J., Swanson, N., Seneff, S., 2015. The High Cost of Pesticides: Human and Animal Diseases. *Poultry,
544 Fisheries & Wildlife Sciences* 03. <https://doi.org/10.4172/2375-446X.1000132>
- 545 Ibrahim, H.M., Alghamdi, A.G., 2021. Effect of the Particle Size of Clinoptilolite Zeolite on Water Content
546 and Soil Water Storage in a Loamy Sand Soil. *Water* 13. <https://doi.org/10.3390/w13050607>
- 547 Jiang, S., Huang, L., Nguyen, T.A.H., Ok, Y.S., Rudolph, V., Yang, H., Zhang, D., 2016. Copper and zinc
548 adsorption by softwood and hardwood biochars under elevated sulphate-induced salinity and
549 acidic pH conditions. *Chemosphere* 142, 64–71.
550 <https://doi.org/10.1016/j.chemosphere.2015.06.079>
- 551 Joshi, V., Srivastava, A., Srivastava, P.C., 2016. Potential of some soil amendments in reducing leaching of
552 fipronil to groundwater. *International Journal of Environmental Science and Technology* 13, 631–
553 638. <https://doi.org/10.1007/s13762-015-0883-1>
- 554 Kookana, R.S., Sarmah, A.K., Van Zwieten, L., Krull, E., Singh, B., 2011. Chapter three - Biochar Application to
555 Soil: Agronomic and Environmental Benefits and Unintended Consequences, in: Sparks, D.L. (Ed.),
556 *Advances in Agronomy*. Academic Press, pp. 103–143. <https://doi.org/10.1016/B978-0-12-385538-1.00003-2>
- 558 Kumari, K.G.I.D., Moldrup, P., Paradelo, M., Elsgaard, L., de Jonge, L.W., 2016. Soil Properties Control
559 Glyphosate Sorption in Soils Amended with Birch Wood Biochar. *Water, Air, & Soil Pollution* 227,
560 174. <https://doi.org/10.1007/s11270-016-2867-2>
- 561 Lahori, A.H., Zhang, Z., Guo, Z., Li, R., Mahar, A., Awasthi, M.K., Wang, P., Shen, F., Kumbhar, F., Sial, T.A.,
562 Zhao, J., Guo, D., 2017. Beneficial effects of tobacco biochar combined with mineral additives on
563 (im)mobilization and (bio)availability of Pb, Cd, Cu and Zn from Pb/Zn smelter contaminated soils.
564 *Ecotoxicology and Environmental Safety* 145, 528–538.
565 <https://doi.org/10.1016/j.ecoenv.2017.07.071>
- 566 Leyva-Ramos, R., Jacobo-Azuara, A., Diaz-Flores, P.E., Guerrero-Coronado, R.M., Mendoza-Barron, J.,
567 Berber-Mendoza, M.S., 2008. Adsorption of chromium(VI) from an aqueous solution on a
568 surfactant-modified zeolite. *Colloids and Surfaces A: Physicochemical and Engineering Aspects* 330,
569 35–41. <https://doi.org/10.1016/j.colsurfa.2008.07.025>
- 570 Liu, G.C., Pan, M.Q., Song, J.Y., Guo, M.Y., Xu, L.N., Xin, Y.J., 2022. Investigating the effects of biochar
571 colloids and nanoparticles on cucumber early seedlings. *Sci Total Environ* 804.
572 <https://doi.org/10.1016/j.scitotenv.2021.150233>
- 573 Liu, Y., 2006. Some consideration on the Langmuir isotherm equation. *Colloids and Surfaces A:
574 Physicochemical and Engineering Aspects* 274, 34–36.
575 <https://doi.org/10.1016/j.colsurfa.2005.08.029>
- 576 Liu, Z., Dugan, B., Masiello, C.A., Gonnermann, H.M., 2017. Biochar particle size, shape, and porosity act
577 together to influence soil water properties. *PLOS ONE* 12, e0179079.
578 <https://doi.org/10.1371/journal.pone.0179079>
- 579 Menezes, D.B., Brazil, O.A.V., Romanholo-Ferreira, L.F., de Lourdes T. M. Polizeli, M., Ruzene, D.S., Silva,
580 D.P., Costa, L.P., Hernández-Macedo, M.L., 2017. Prospecting fungal ligninases using corncob
581 lignocellulosic fractions. *Cellulose* 24, 4355–4365. <https://doi.org/10.1007/s10570-017-1427-2>
- 582 Mohan, D., Abhishek, K., Sarswat, A., Patel, M., Singh, P., Pittman, C.U., 2018. Biochar production and
583 applications in soil fertility and carbon sequestration – a sustainable solution to crop-residue
584 burning in India. *RSC Adv.* 8, 508–520. <https://doi.org/10.1039/C7RA10353K>

585 Mondal, M., Biswas, B., Garai, S., Sarkar, S., Banerjee, H., Brahmachari, K., Bandyopadhyay, P.K., Maitra, S.,
586 Brestic, M., Skalicky, M., Ondrisik, P., Hossain, A., 2021. Zeolites Enhance Soil Health, Crop
587 Productivity and Environmental Safety. *Agronomy* 11. <https://doi.org/10.3390/agronomy11030448>
588 Ramos, C.G., Querol, X., Oliveira, M.L.S., Pires, K., Kautzmann, R.M., Oliveira, L.F.S., 2015. A preliminary
589 evaluation of volcanic rock powder for application in agriculture as soil a remineralizer. *Sci Total*
590 *Environ* 512–513, 371–380. <https://doi.org/10.1016/j.scitotenv.2014.12.070>
591 Ritter, W.F., 1988. Reducing Impacts of Nonpoint Source Pollution from Agriculture - a Review. *J Environ Sci*
592 *Heal A J Environ Sci Heal A* 23, 645–667.
593 Sarabi, S., Sepaskhah, A., 2012. Effect of zeolite and saline water application on saturated hydraulic
594 conductivity and infiltration in different soil textures. *Archives of Agronomy and Soil Science* 59, 1–
595 12. <https://doi.org/10.1080/03650340.2012.675626>
596 Schmidt, H.-P., 2015. European Biochar Certificate (EBC) - guidelines version 6.1.
597 <https://doi.org/10.13140/RG.2.1.4658.7043>
598 Sethi, R., Di Molfetta, A., 2019. GROUNDWATER ENGINEERING A Technical Approach to Hydrogeology,
599 Contaminant Transport and Groundwater Remediation. [https://doi.org/10.1007/978-3-030-20516-](https://doi.org/10.1007/978-3-030-20516-4)
600 4
601 Shan, D., Deng, S., Zhao, T., Wang, B., Wang, Y., Huang, J., Yu, G., Winglee, J., Wiesner, M.R., 2016.
602 Preparation of ultrafine magnetic biochar and activated carbon for pharmaceutical adsorption and
603 subsequent degradation by ball milling. *Journal of Hazardous Materials* 305, 156–163.
604 <https://doi.org/10.1016/j.jhazmat.2015.11.047>
605 Silveira, M.L., Alleoni, L.R.F., O'Connor, G.A., Chang, A.C., 2006. Heavy metal sequential extraction
606 methods—A modification for tropical soils. *Chemosphere* 64, 1929–1938.
607 <https://doi.org/10.1016/j.chemosphere.2006.01.018>
608 Simunek, J., Jacques, D., Langergraber, G., Bradford, S.A., Sejna, M., van Genuchten, M.T., 2013. Numerical
609 Modeling of Contaminant Transport Using HYDRUS and its Specialized Modules. *J Indian I Sci* 93,
610 265–284.
611 Simunek, J., van Genuchten, M.T., Sejna, M., 2012. Hydrus: Model Use, Calibration, and Validation. *T Asabe*
612 55, 1261–1274.
613 Sud, D., Mahajan, G., Kaur, M.P., 2008. Agricultural waste material as potential adsorbent for sequestering
614 heavy metal ions from aqueous solutions – A review. *Bioresource Technology* 99, 6017–6027.
615 <https://doi.org/10.1016/j.biortech.2007.11.064>
616 Tan, X., Liu, Y., Zeng, G., Wang, X., Hu, X., Gu, Y., Yang, Z., 2015. Application of biochar for the removal of
617 pollutants from aqueous solutions. *Chemosphere* 125, 70–85.
618 <https://doi.org/10.1016/j.chemosphere.2014.12.058>
619 Tong, Y., McNamara, P.J., Mayer, B.K., 2019. Adsorption of organic micropollutants onto biochar: a review
620 of relevant kinetics, mechanisms and equilibrium. *Environ. Sci.: Water Res. Technol.* 5, 821–838.
621 <https://doi.org/10.1039/C8EW00938D>
622 Tran, H., You, S.-J., Chao, H.-P., 2015. Effect of pyrolysis temperatures and times on the adsorption of
623 cadmium onto orange peel derived biochar. *Waste Management & Research* 34.
624 <https://doi.org/10.1177/0734242X15615698>
625 Vadivelan, V., Kumar, K.V., 2005. Equilibrium, kinetics, mechanism, and process design for the sorption of
626 methylene blue onto rice husk. *Journal of Colloid and Interface Science* 286, 90–100.
627 <https://doi.org/10.1016/j.jcis.2005.01.007>
628 Verheijen, F.G.A., Zhuravel, A., Silva, F.C., Amaro, A., Ben-Hur, M., Keizer, J.J., 2019. The influence of biochar
629 particle size and concentration on bulk density and maximum water holding capacity of sandy vs
630 sandy loam soil in a column experiment. *Geoderma* 347, 194–202.
631 <https://doi.org/10.1016/j.geoderma.2019.03.044>
632 Wang, J., Chen, T., Li, S., Yue, Z.-B., Jin, J., He, G., Zhang, H., 2012. Biosorption of Copper (II) from Aqueous
633 Solutions with Rape Straw. *Geomicrobiology Journal* 29, 250–254.
634 <https://doi.org/10.1080/01490451.2011.598603>

- 635 Wang, S.Z., Wang, J.L., 2022. Magnetic 2D/2D oxygen doped g-C₃N₄/biochar composite to activate
636 peroxymonosulfate for degradation of emerging organic pollutants. *J Hazard Mater* 423.
637 <https://doi.org/10.1016/j.jhazmat.2021.127207>
- 638 Waqas, M., Asam, Z.-Z., Rehan, M., Anwar, M., Khattak, R., Ismail, I., Tabatabaei, M., Nizami, Dr.A.-S., 2021.
639 Development of biomass-derived biochar for agronomic and environmental remediation
640 applications. *Biomass Conversion and Biorefinery* 11, 1–23. <https://doi.org/10.1007/s13399-020-00936-2>
- 642 Yan, Y., Akbar Nakhli, S.A., Jin, J., Mills, G., Willson, C.S., Legates, D.R., Manahiloh, K.N., Imhoff, P.T., 2021.
643 Predicting the impact of biochar on the saturated hydraulic conductivity of natural and engineered
644 media. *Journal of Environmental Management* 295, 113143.
645 <https://doi.org/10.1016/j.jenvman.2021.113143>
- 646 Zand, A.D., Abyaneh, M.R., 2020. Adsorption of Lead, manganese, and copper onto biochar in landfill
647 leachate: implication of non-linear regression analysis. *Sustainable Environment Research* 30, 18.
648 <https://doi.org/10.1186/s42834-020-00061-9>
- 649 Zhao, S., Ta, N., Wang, X., 2020. Absorption of Cu(II) and Zn(II) from Aqueous Solutions onto Biochars
650 Derived from Apple Tree Branches. *Energies* 13. <https://doi.org/10.3390/en13133498>
- 651 Zou, W., Han, R., Chen, Z., Jinghua, Z., Shi, J., 2006. Kinetic study of adsorption of Cu(II) and Pb(II) from
652 aqueous solutions using manganese oxide coated zeolite in batch mode. *Colloids and Surfaces A:
653 Physicochemical and Engineering Aspects* 279, 238–246.
654 <https://doi.org/10.1016/j.colsurfa.2006.01.008>
- 655

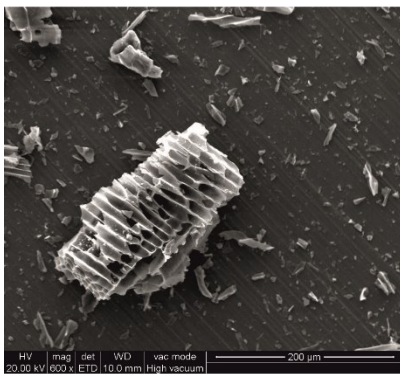
656 **Acknowledgements**

657 The authors thank prof. Rajandrea Sethi for guidance and support in the study development.

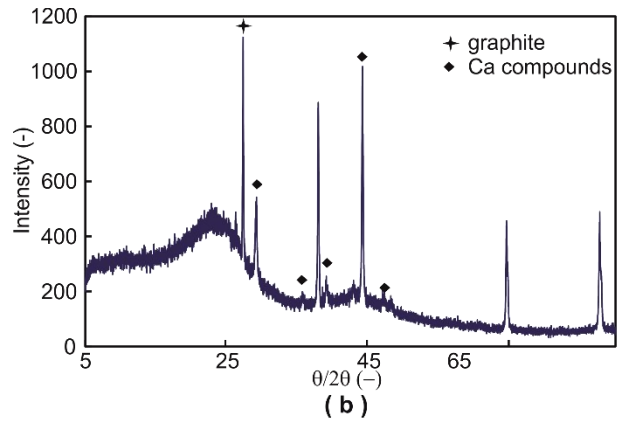
658 The part of the study concerning corncob has received funding in the framework of the project NODES from
659 the MUR - M4C2 1.5 of PNRR funded by the European Union - NextGenerationEU (Grant agreement no.
660 ECS00000036).

661

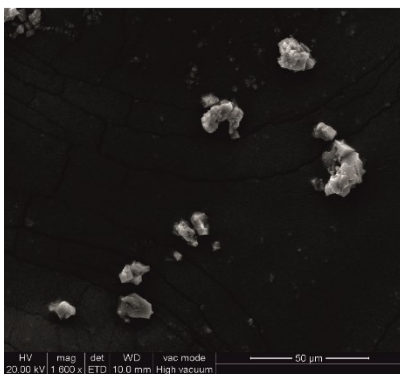
662



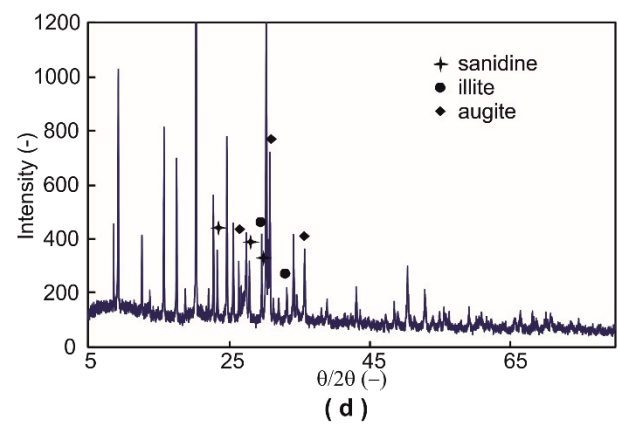
(a)



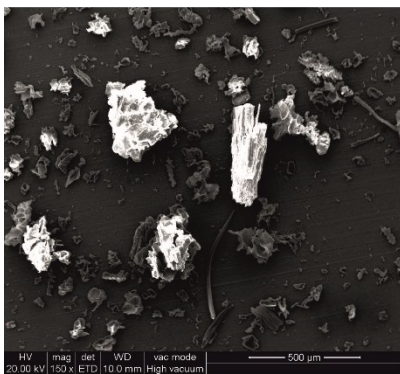
(b)



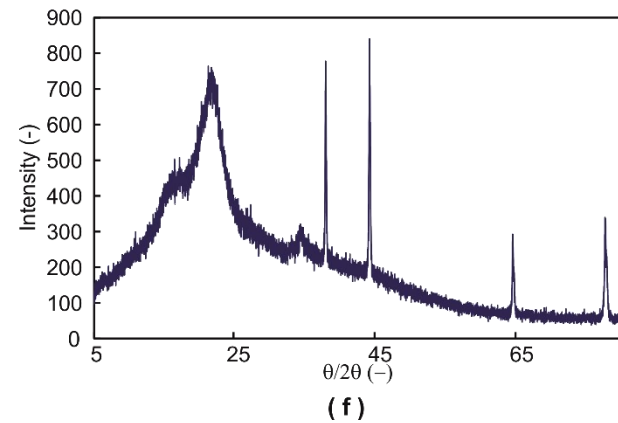
(c)



(d)



(e)

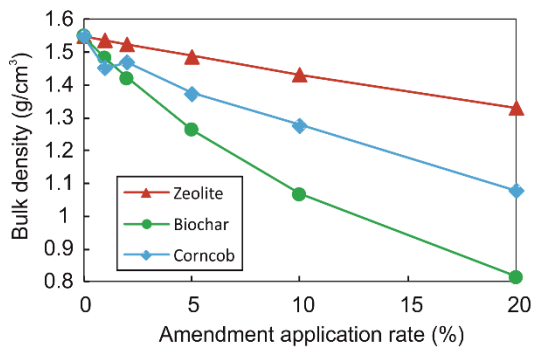


(f)

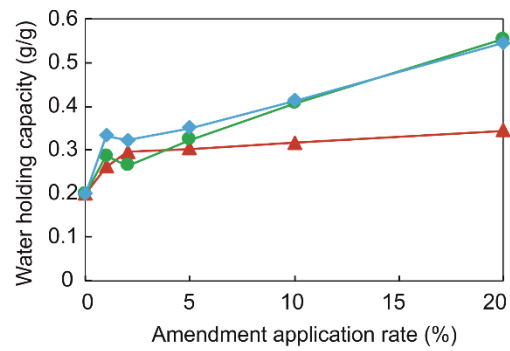
664

665 Figure 1 SEM images (a, c, e) and XRD spectra (b, d, f) for biochar (a, b), zeolite (c, d) and corncob (e, f) samples.

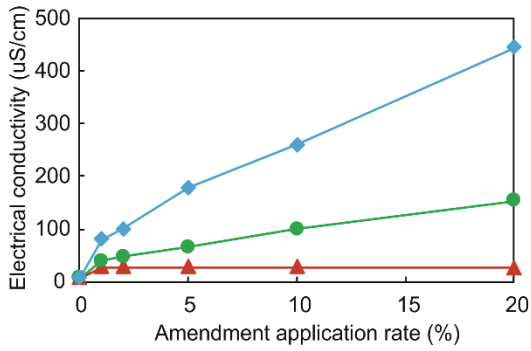
666



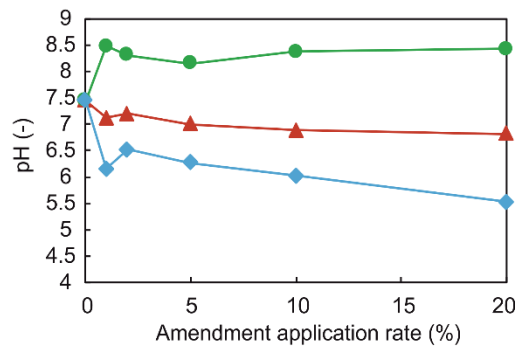
(a)



(b)



(c)

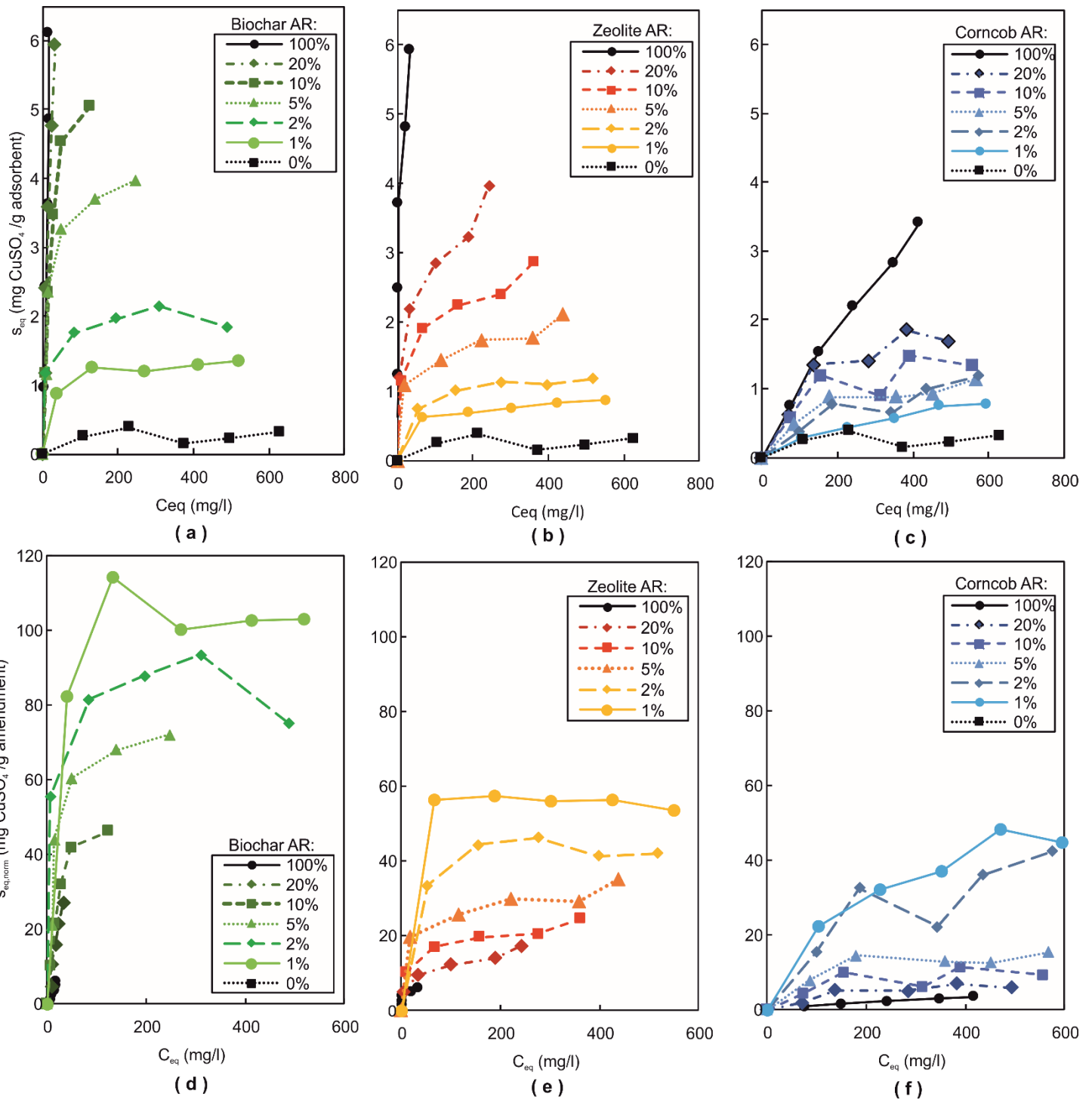


(d)

667

668 *Figure 2 Bulk density (a), water holding capacity (b), electrical conductivity (c) and pH (d) for amendment-*
 669 *sand mixtures at different application rates*

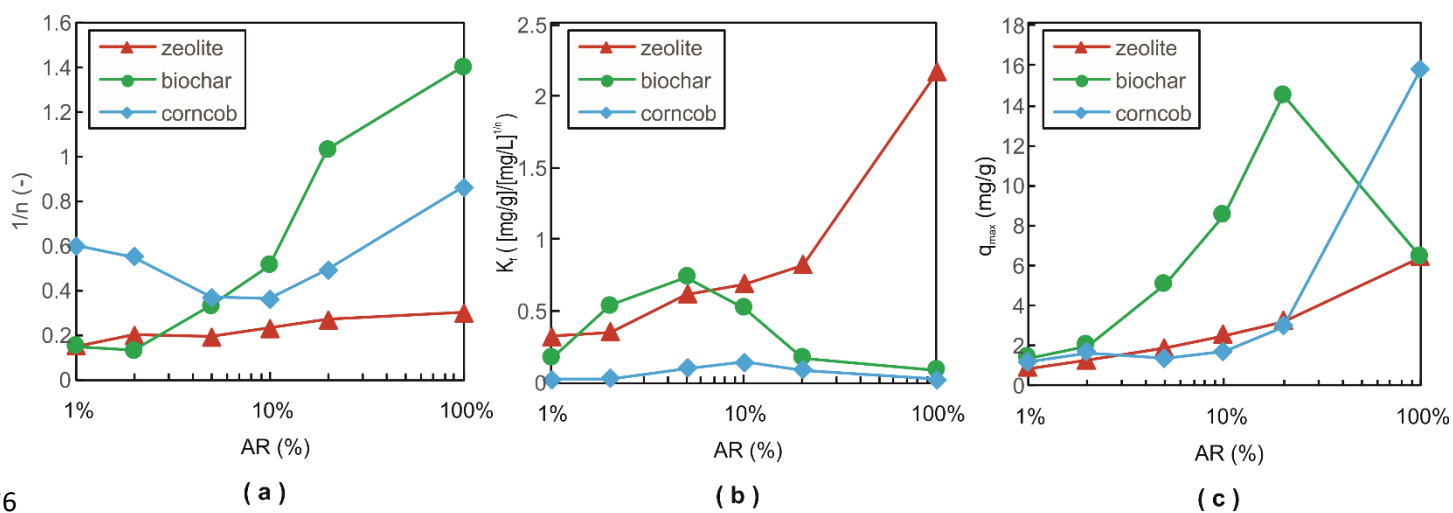
670



671

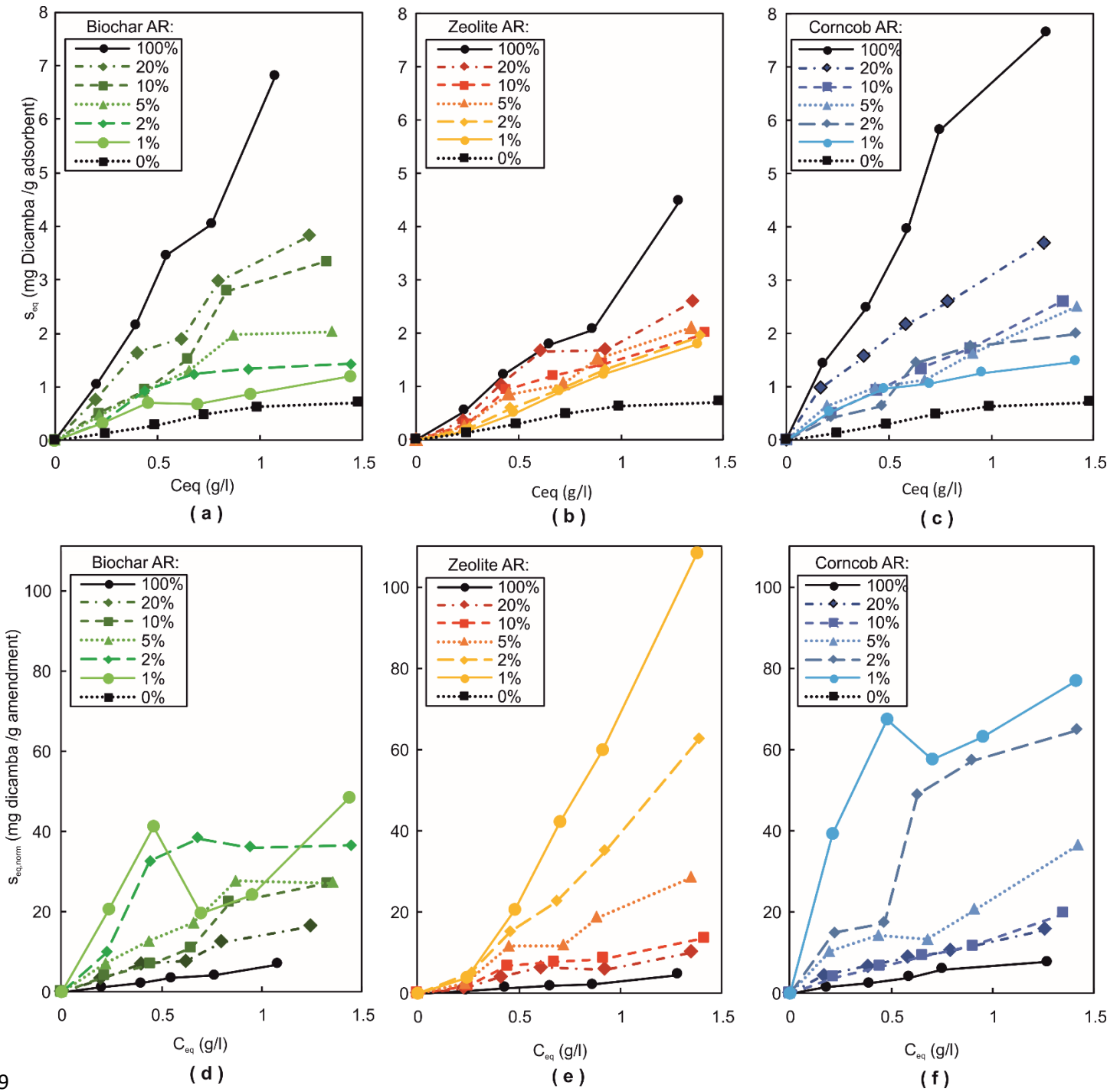
672 *Figure 3 Copper sulphate adsorption isotherms reported as adsorbed $CuSO_4$ per total mass of adsorbent (sand*
 673 *+ amendment) (a-c) and per total mass of amendment (d-f) vs equilibrium concentration in liquid phase, at*
 674 *different application rates (AR), for biochar (a,d), zeolite (b,e) and corncob (c,f)*

675



676

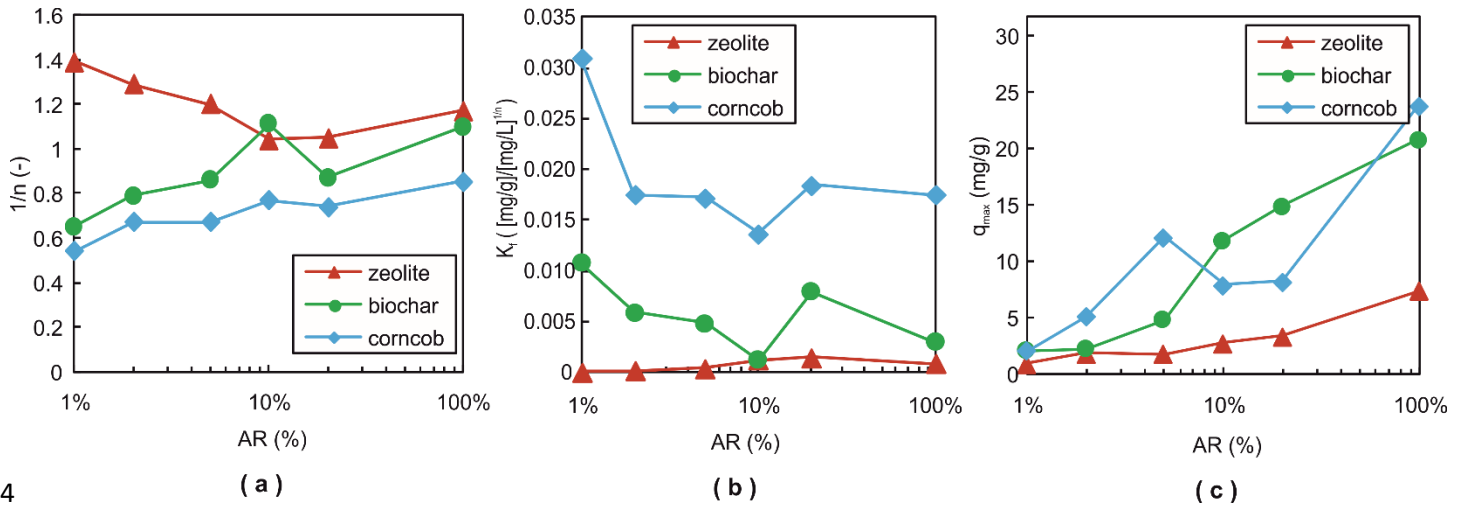
677 *Figure 4 Freundlich (a,b) and Langmuir (c) parameters for CuSO_4 adsorption isotherms as a function of the*
 678 *amendment application rate*



679

680 *Figure 5 Dicamba adsorption isotherms reported as adsorbed dicamba per total mass of adsorbent (sand +*
 681 *amendment) (a-c) and per total mass of amendment (d-f) vs equilibrium concentration in liquid phase, at*
 682 *different application rates (AR), for biochar (a,d), zeolite (b,e) and corncob (c,f)*

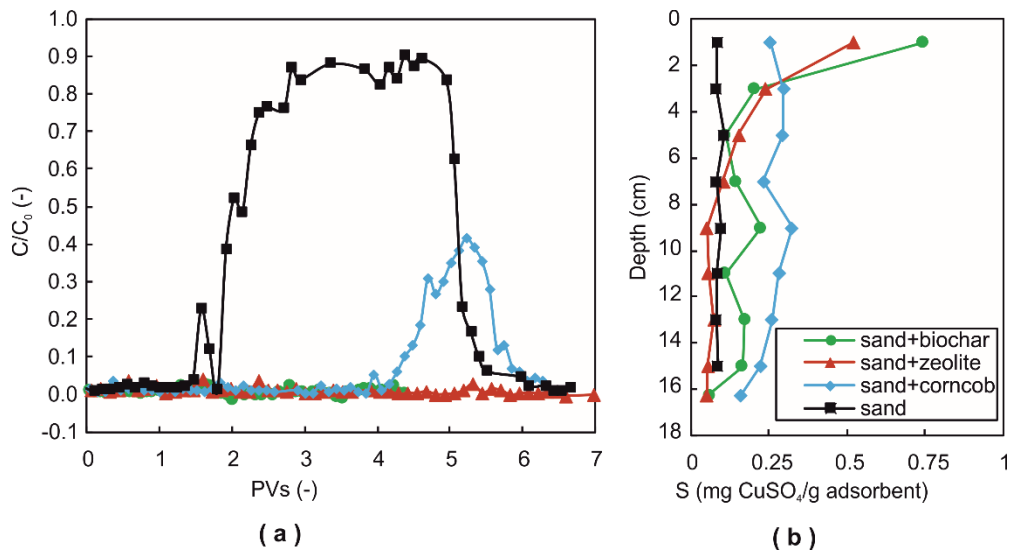
683



684

685 *Figure 6 Freundlich (a,b) and Langmuir (c) parameters for dicamba adsorption isotherms as a function of the*
 686 *amendment application rate*

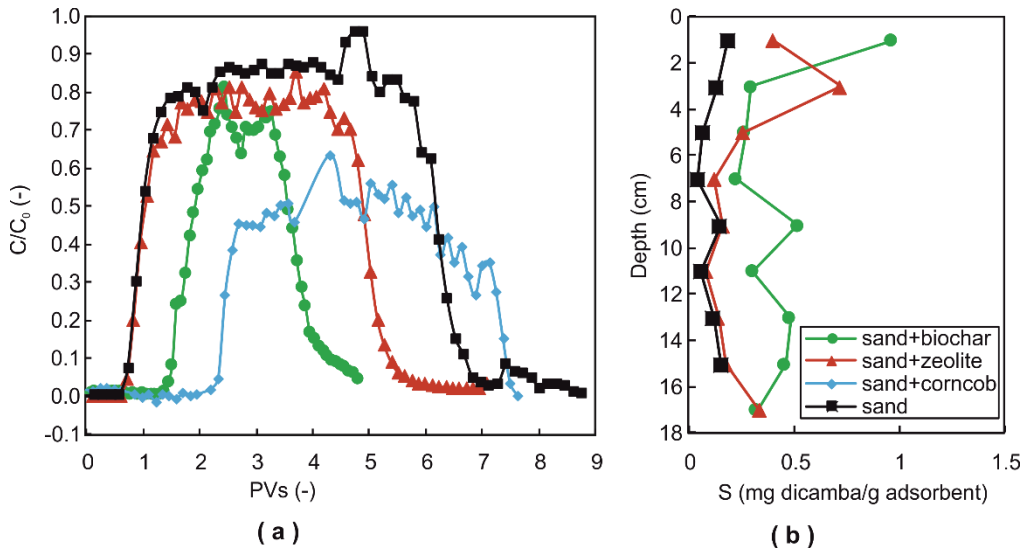
687



688

689 *Figure 7 Normalized $CuSO_4$ breakthrough curve (C/C_0 as a function of the number of injected pore volumes*
 690 *PVs) (a) and final vertical profile of adsorbed $CuSO_4$ (mass concentration S versus depth) (b) for sand and sand-*
 691 *amendment column leaching tests. The injection starts at PV = 0 (column pre-conditioning and tracer tests*
 692 *are not reported)*

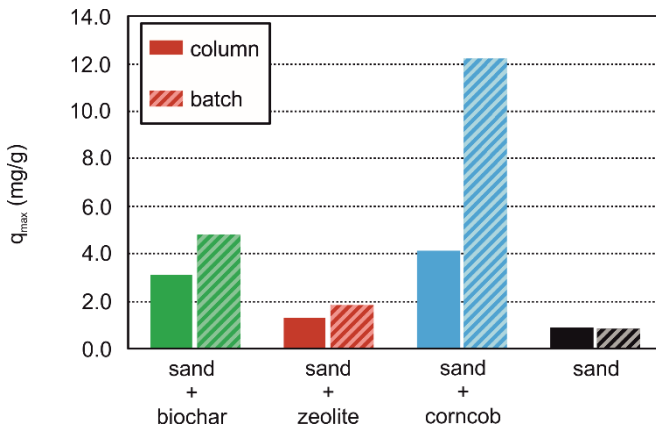
693



694

695 *Figure 8 Normalized dicamba breakthrough curve (C/C_0 as a function of the number of injected pore volumes*
 696 *PVs) (a) and final vertical profile of adsorbed dicamba(mass concentration S versus depth) (b) for sand and*
 697 *sand-amendment column leaching tests. The injection starts at PV = 0 (column pre-conditioning and tracer*
 698 *tests are not reported)*

699



700

701 *Figure 9 Comparison of maximum adsorption capacity q_{max} obtained via fitting of breakthrough curves of*
 702 *column transport tests (solid bars) and of adsorption isotherms of batch tests (dashed bars) of dicamba*
 703 *solutions in contact with sand-amendment mixtures (application rate equal to 5%) and pure sand.*

704

705 **TABLE CAPTION**706 *Table 1 Column leaching tests: geometrical characteristics, hydrodynamic parameters and mass balance*
707 *results*

708

	Sand	Zeolite-sand	Biochar-sand	Corncob-sand
CuSO₄				
Column length (cm)	15	16.5	18	18
Bulk density (g/cm³)	1.54	1.40	1.28	1.28
Porosity (-)	0.41	0.42	0.485	0.44
Pore volume PV (min)	132	117	193	142
Unsaturated water content (-)	0.22	0.216	0.32	0.23
Saturated hydraulic conductivity K_{sat} (m/s)	7.92·10 ⁻⁵	5.72·10 ⁻⁵	2.59·10 ⁻⁵	5.88·10 ⁻⁵
Hydrodynamic dispersivity α (m)	4.16·10 ⁻³	5.38·10 ⁻³	5.99·10 ⁻³	2.85·10 ⁻³
Leached CuSO₄ (%)	56	1.2	1.1	10.2
Recovered CuSO₄ (leached + extracted) (%)	101.4	37.7	53.4	75.6
Dicamba				
Column length (cm)	15.4	17	18.2	18.5
Bulk density (g/cm³)	1.50	1.36	1.27	1.25
Porosity (-)	0.40	0.41	0.48	0.44
Pore volume PV (min)	101	125	197	122
Unsaturated water content (m³/m³)	0.19	0.21	0.31	0.2
Saturated hydraulic conductivity K_{sat} (m/s)	1.01·10 ⁻⁴	6.32·10 ⁻⁵	2.70·10 ⁻⁵	9·10 ⁻⁵
Hydrodynamic dispersivity α (m)	4.67·10 ⁻³	4.34·10 ⁻³	4.32·10 ⁻³	7.58·10 ⁻³
Leached dicamba (%)	87	70	45.4	44
Recovered dicamba (leached + extracted) (%)	99	98.1	45.4*	88.9

709 * Dicamba vertical profile was not determined